Geomorphology 243 (2015) 51–64

Contents lists available at ScienceDirect

Geomorphology

journal homepage: www.elsevier.com/locate/geomorph

Formation processes, geomechanical characterisation and buttressing effects at the toe of deep-seated rock slides in foliated metamorphic rock

C. Zangerl [a,b,*], W. Chwatal [c], H. Kirschner [b,d]

[a] Department of Civil Engineering and Natural Hazards, Institute of Applied Geology, University of Natural Resources and Life Sciences, Peter Jordan-Strasse 70, A-1190 Vienna, Austria
[b] alpS GmbH, Grabenweg 68, A-6020 Innsbruck, Austria
[c] Department of Geodesy and Geoinformation, Vienna University of Technology, 1040 Vienna, Austria
[d] Geo-Engineering HKi, A-6020 Innsbruck, Austria

ARTICLE INFO

Article history:
Received 2 September 2014
Received in revised form 13 March 2015
Accepted 14 March 2015
Available online 16 April 2015

Keywords:
Deep-seated rock slides
Fractured metamorphic rock mass
Numerical modelling
Buttressing effects

ABSTRACT

In order to increase the understanding of deep-seated rock slides in terms of formation processes, kinematics, and the impact of geometrical factors on slope stability and deformation behaviour, a 300 m thick active rock slide located in Austria was investigated. Results of geological and geodetic field surveys, geophysical in-situ investigations and numerical modelling are presented and analysed. Particular focus is given on the geomechanical characterisation of the rock slide mass, progressive topographical slope changes due to initial rock slide formation processes, internal rock mass deformation processes and back-calculated strength properties of the basal shear zone. Back calculations considering the actual rock slide geometry yields a friction angle of the basal shear zone of about 24°. Rock slide volume balance analyses are performed in order to determine mass loss due to secondary slides and river erosion. In relation to the pre-failure topography, the middle to upper part of the rock slide has lost (zone of depletion) and the foot of the slope has accumulated rock mass material (zone of accumulation). GIS-based estimations show an enormous volume imbalance between the depletion and accumulation zones. Given that the volume accumulation at the foot of the slope is nearly three times smaller than the volume depletion at higher elevations, considerable erosion of the toe by the river has occurred. The complex geological interaction of the rock slide with the alluvium at the toe of the slope was a key question of this study, and thus the geomechanical impact of the alluvium on slope deformation and stability behaviour was studied by applying 2D discrete element modelling methods. Results show that the alluvium at the foot of the slope has a positive effect on the slope stability and the sensitivity of the stability behaviour.

1. Introduction

The mechanisms and processes that cause fracturing, fragmentation, and internal deformation of rock masses and the initial formation of failure and shear zones of very slow deep-seated rock slides in foliated metamorphic rock are still not fully understood (Cruden and Varnes, 1996). New models focusing on these geomechanical processes need to be established. Analyses of post-failure rock slide geometries in relation to pre-failure slope topographies and surface deformation monitoring as well as subsurface investigation data (e.g. boreholes, seismic surveys, inclinometers) help to obtain new fundamental information about these complex slope processes.

It is frequently observed that deep-seated rock slides experience considerable changes in their geometry in the course of their development and deformation history. Numerous field observations of rock slides which developed in metamorphic rock (e.g. schists, paragneisses, and phyllites) show considerable changes between the pre-failure slope topography and the post-failure one (Bonzanigo et al., 2007). The characteristics of post-failure slope geometries is usually a convex shaped i.e. bulge-like topography at the foot of the slope and a concave shaped i.e. subsidence-like topography in the middle to upper part. Field surveys show that the newly formed slope geometries result from gravitational slope processes where overall internal rock mass deformation has occurred within the slide. Cataclasis, fracturing, shearing and dilatation are the key deformation processes. Analyses of cored drillings from deep-seated slides in similar metamorphic rock masses (i.e. mica schist and paragneiss) show relative to the stable bedrock underneath an increased density of brittle shear zones (i.e. fault gouges and breccias) and meso-scale fractures (Bonzanigo et al., 2007; Watson et al., 2007; Agliardi et al., 2009, 2012; Barla, 2010; Zangerl et al., 2010a,b). The increased fragmentation and loosening of the rock mass predominately results from internal rock mass strains, most likely initiated during the first-time rock slide formation process.

A slope deformation mechanism which is often observed during the initial formation process of rock slides is toppling which can penetrate

* Corresponding author at: Department of Civil Engineering and Natural Hazards, Institute of Applied Geology, University of Natural Resources and Life Sciences, Peter Jordan-Strasse 70, A-1190 Vienna, Austria. Tel.: +43 1 47654 5414; fax: +43 1 47654 5449.
E-mail address: christian.j.zangerl@boku.ac.at (C. Zangerl).

http://dx.doi.org/10.1016/j.geomorph.2015.03.030
0169-555X/

deeply into the rock mass. It is also observed that this type of failure mechanism is linked to geological structures (i.e. foliation, joints and fault planes) which are dipping steeply into the slope and thus are prone to toppling. Whereas in some cases the toppling activity is advancing at slow rates or comes to a halt, others are characterised by a transition from toppling to sliding kinematics (Zischinsky, 1969; Guglielmia et al., 2000; Amann, 2006). In this situation a basal shear zone is newly formed along the inflexion points of the rock strata at great depths. A case study exemplarily for such slope behaviour is the well known La Clapiere rock slide in France (Guglielmia et al., 2000; Helmstetter et al., 2004).

However, rock mass fracturing and deformation processes which cause internal rock mass fragmentation, strain localisation and finally the formation of basal shear zones are still poorly understood. As a hypothesis, internal rock mass deformation may result from advanced toppling processes (Sjörberg, 2000) or from increased internal rock mass straining. Later on, ongoing slope deformations lead to strain localization and subsequently to the formation of discrete shear zones at the base of the slide and inside of the rock mass. Along these shear zones most of the actually measured slope displacement takes place (Noverraz, 1996) and sliding becomes the final slope deformation process. This has been proven by numerous inclinometer measurements in active rock slides (Noverraz, 1996; Watson et al., 2007; Zangerl et al., 2010a). Often the measurements show that separate blocks or rafts of blocks in between the active shear zones experience either no or only minor strain and thus are dominated by en bloc movement.

The consequences of internal rock mass deformation processes on slope behaviour are manifold. Firstly, strain localization leads to the formation of one or several discrete shear zones composed of fault breccias and gouges (similar to tectonically formed fault zones) which control the deformation and strength behaviour (Zangerl et al., 2009). Secondly, internal rock mass strains can change the sliding mass geometry considerably and thus affect the in-situ stress condition along the active sliding zone(s). Thirdly, the internal deformation process causes rock cataclasis, fracturing and fragmentation which reduces the strength of the rock mass and alters its hydrogeological properties (i.e. increasing porosity, permeability and storativity). This can favour the formation of secondary rock slides at the toe of large rock slide systems.

In order to increase the fundamental understanding of formation processes, the impact of geometrical factors on slope stability and deformation behaviour, and the kinematics of deep-seated rock slides in general, the 300 m thick Niedergallmigg rock slide in Austria was investigated in great detail. Particular focus is given on the geomechanical characterisation of the rock slide mass, progressive topographical slope changes due to initial rock slide formation processes, internal rock mass deformation processes and back-calculated strength properties of the basal shear zone. The complex geological interaction of the rock slide with the alluvium at the toe of the slope was investigated and the mechanical impact of the alluvium on slope deformation and stability behaviour was studied by using 2D numerical modelling methods. Furthermore, rock slide volume balance analyses are performed in order to determine mass loss due to secondary slides and river erosion.

2. Geological and hydrogeological setting

The Niedergallmigg rock slide is located in Northern Tyrol, Austria (ETRS89 10°37′29″ / 47°06′38″, Zangerl et al., 2012). It has a difference in elevation between the toe where the River Inn is located and the main scarp of about 1400 m and a maximum E–W extension of almost 1500 m (Figs. 1 and 2). Morphological features, in particular the location of the main scarp just under the summit of the Matekopf (2248 ma.s.l) indicate a total displacement of the rock slide mass of at least 200 m (Fig. 1). The large slope displacements caused the formation of a remarkably well-shaped main scarp as well as left and right flanks which are traceable across the entire slope. The pre-failure mean slope inclination was around 30°.

Tectonostratigraphically, the rock slide is situated within the Silvretta Crystalline Complex which comprises the upper part of it (Fig. 3; Brandner, 1980). The middle to lower part of the slide consists of strata belonging to the Landecker Quartzphyllite Zone. The main thrust fault between these two main tectonostratigraphic units is flatly dipping and outcrops at an elevation between 1500 and 1600 ma.s.l. (Fig. 3). Hence the paragneisses and schists of the Silvretta Crystalline were thrust over the phyllitic gneisses and phyllites of the Landecker Quarzphyllite Zone. In the study area the NE–SW trending Engadine and the E–W trending Inn Valley Fault Zone are the main structural lineaments in a strike-slip mode. Within the units, polyphase deformation processes formed ductile and brittle structures that influence the rock mass strength and anisotropy. Based on aerial views, digital terrain models from airborne laser scanning and field surveys E–W striking steeply dipping fault zones were found to be the dominant structures in the area mapped (Fig. 1). These structures dissect the rock mass into E–W striking platy-shaped blocks which are prone to toppling towards the north under stress release conditions.

The meso-scale fracture network in the scarp area (Fig. 4) is dominated by two steeply inclined joint sets, one striking NE–SW with a mean dip direction/dip angle of 136°/84° (Joint set JS1) and another one striking NW–SE showing a mean dip direction and dip angle of 209°/81° (Joint set JS2). In addition, two intermediately inclined joint sets dipping NE (Joint set JS3; dip direction and dip angle of 42°/54°) and W (Joint set JS4; dip direction and dip angle of 264°/45°), respectively, were observed. In the scarp area a dominantly and favourably oriented joint set sub-parallel to the basal shear zone of the rock slide was not observed. However, at local scale a few joints can be aligned sub-parallel to the basal shear zone of the rockslide.

In the upper part of the slope i.e. within the Silvretta Crystalline Complex, foliation planes are nearly flat i.e. at a mean dip direction/dip angle of 126°/04° (Fig. 4). Within the Landecker Quartzphyllite Zone, in the lower part of the slope, the foliation dips moderately to the south and therefore into the slope (Fig. 4). Based on statistical analyses a mean dip direction and dip angle of 172°/60° was determined. Similar to other geological structures the foliation was oriented unfavourably to favour slope failure in a simple dip-slope sliding mode. As opposed to other case studies in similar rock types, the structural inventory does not indicate the presence of fracture sets which are aligned sub-parallel to the slope and would therefore favour the formation of a coherent basal shear zone (Zangerl and Prager, 2008). In contrast, some of these structures, especially the steeply inclined brittle fault zones, joints and foliation planes favour toppling processes.

Glacial and fluvial processes have caused deep erosion of the valley which was subsequently filled with alluvium i.e. fluvial soils (silt, sand and gravel, Fig. 3). A detailed depiction of the geomorphological situation at the toe of the slide is given in Fig. 5. The formation and ongoing movement of the Niedergallmigg rock slide have compressed these sediments and formed a gorge-like relief in the bedrock. Based on unpublished seismic investigations and borehole data obtained for an investigation of a power supply weir located further east, an alluvium thickness of at least 100 m is assumed in the rock slide area. The lack of borehole data directly at the foot of the Niedergallmigg rock slide does not enable a detail study about the complex interplay between alluvial sedimentation processes and ongoing rock slide deformation.

Generally, due to deficiency of subsurface investigations e.g. the installation of piezometers, the groundwater system of the Niedergallmigg rock slide is poorly understood. So far only spring and stream mapping data are available, which roughly show a major spring line between 1000 and 1300 ma.s.l. (Fig. 3). Surrounding the rock slide mass, springs are also located at higher elevation levels. Rock mass porosity estimations (11 to 33%, see below) based on seismic investigations suggest the presence of a highly permeable rock slide body with intercalations of less permeable gouge-rich shear zones.

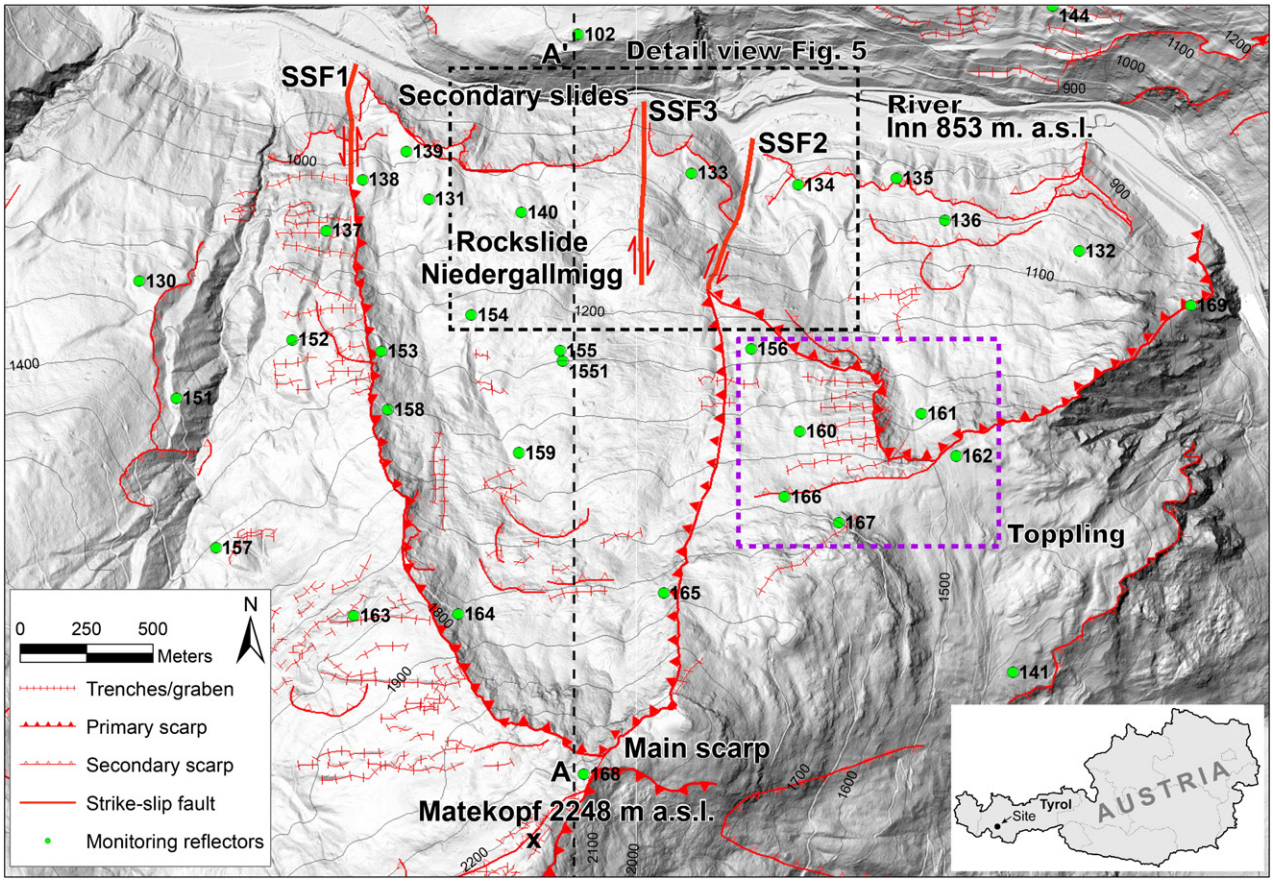

Fig. 1. Airborne laser scanning (LiDAR) based hillshade map of the study site showing primary and secondary scarps of the rock slide, locations of geodetic survey points, strike-slip faults (SSF1, SSF2, and SSF3) at the toe, the trace of the cross section A–A′, and the area characterized by deep-seated toppling processes outside of the slide. LiDAR data are processed to a 1 m raster digital terrain model and are characterised by a position accuracy of ±15 cm and an elevation accuracy of ±30 cm, respectively (data source: Amt der Tiroler Landesregierung, Geoinformation).

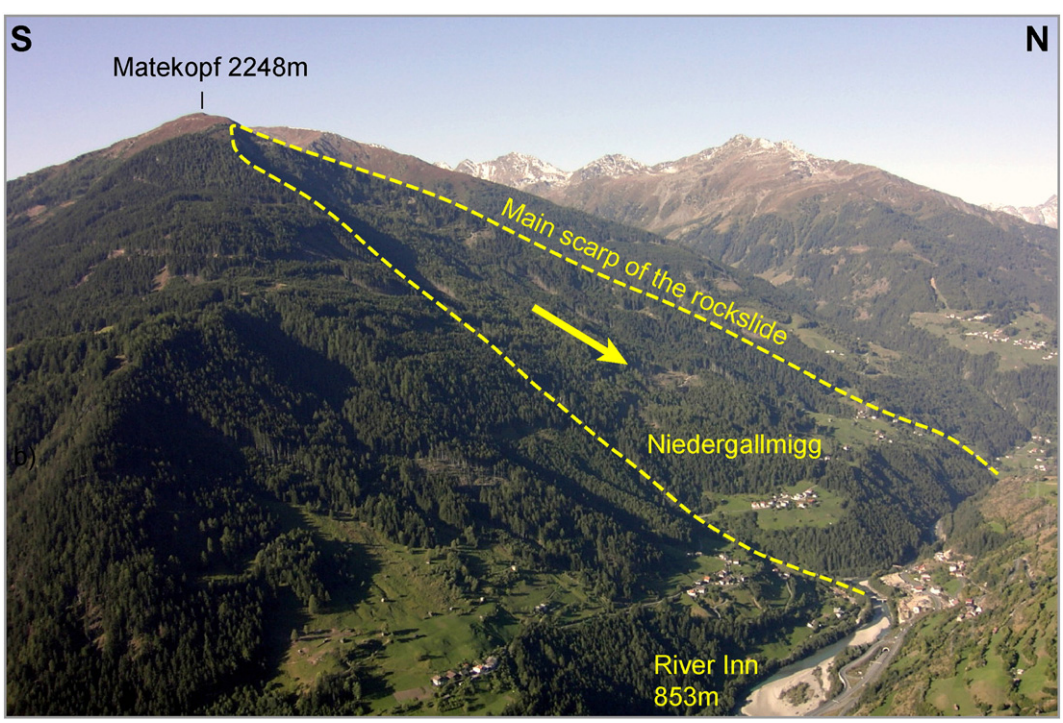

Fig. 2. Overview of the rock slide Niedergallmigg showing the main head scarp, the River Inn and the location of Niedergallmig Village (Tyrol, Austria).

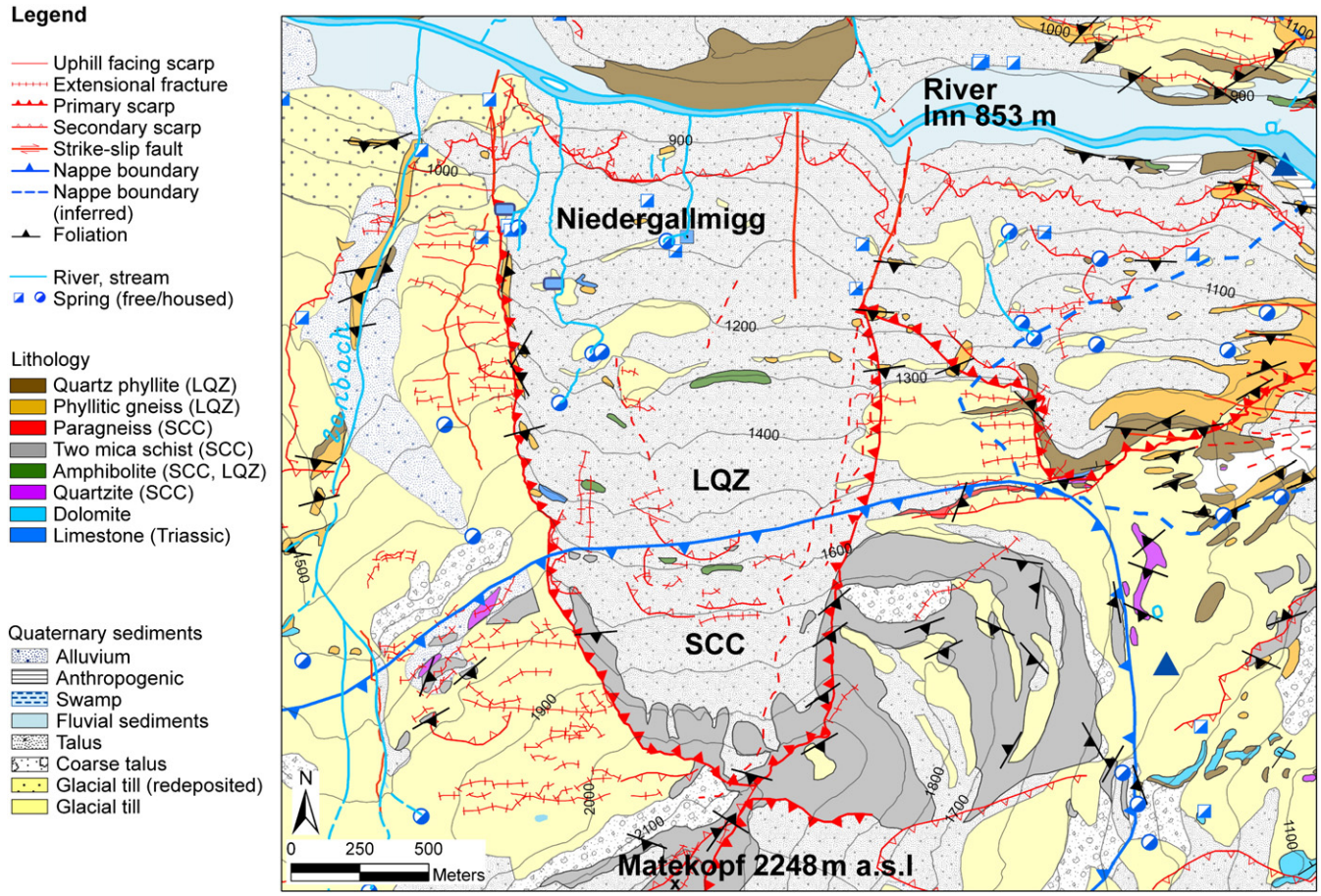

Fig. 3. Geological map depicting lithological rock types, main tectonic units, springs of the study area and the main head scarp of the rock slide. LQZ: Landecker Quartzphyllite Zone, SCC: Silvretta Crystalline Complex.

The electrical conductivity of the spring water varies between 200 and 600 μS cm^{-1} and the temperature between 4 °C and 8 °C, respectively. Hydrochemical analyses indicate the presence of Ca-Mg-HCO_3-SO_4 and Mg-Ca-HCO_3-SO_4 water types. The source of SO_4-rich water is related to the dissolution of gypsum which outcrops at the contact between the Landecker Quarzphyllite Zone and the Silvretta Crystalline Complex (Fig. 3).

3. Seismic investigation

In order to explore the thickness, internal structure and velocity distribution of the rock slide and its surroundings a comprehensive 3-D refraction seismic survey was carried out (Fig. 6; Chwatal et al., 2006; Zangerl et al., 2009). In all 373 seismic stations were installed along 4 transverse profiles comprising a total length of 7.5 km with a geophone distance of 15–25 m. 41 shots were recorded simultaneously by the receivers. This geophone set up enabled 2-D analyses to be done along the 4 profiles but also a 3-D inversion of the whole data set (inline and cross-line shots). For this study a combination of seismic refraction tomography for the rock slide mass and standard seismic refraction method for the compact bedrock was applied. In order to analyse the measured data, 3-D processing techniques (Brückl et al., 2003) and a tomographic inversion algorithm (Hole, 1992) were applied. As a result, the 3-D seismic velocity distribution of the landslide system and its stable surrounding is obtained.

The seismic data show a vertical gradient in the velocity for the sliding mass and a nearly constant velocity for the underlying in-situ and stable bedrock. P-wave velocities of the sliding mass near the surface are 1000–2000 m s^{-1}, at depths of 25–150 m, 2000–3000 m s^{-1} and below 150 m 3000–4000 m s^{-1}. Below 150 m velocities of 4800–5200 m s^{-1} were measured, which are interpreted as the bedrock below the base of the rock slide (Fig. 6). Based on seismic data, a rock slide thickness map showing a maximum thickness of about 320 m was determined (Zangerl et al., 2012). Plotting the P-wave velocities of the sliding mass versus depth, an average velocity-depth relationship was obtained (Chwatal et al., 2006):

$$V_p = 460d^{0.3783} \quad (1)$$

where V_p is *P*-wave velocity [m s^{-1}], and *d* is depth [m].

The porosity of the fractured rock mass based on P-wave velocities and the assumption of dry or drained rock mass conditions was estimated using an empirical relationship of Watkins et al. (1972). For the Niedergallmigg rock slide an average rock mass porosity of 17% was calculated. Within the rock slide mass the porosity varies between 11% at the base and 33% near the surface. This relationship lies in the range of other case studies e.g. the Hochmais, Köfels, Gradenbach and Lesachriegel rock slides (Brückl and Parotidis, 2005; Fig. 7). Average velocity-depth functions show mean porosity variations between 17% and 27%.

4. Slope deformation measurements

In the Niedergallmigg rock slide area, geodetic measurements have been carried out since 1975. The first geodetic campaign was performed

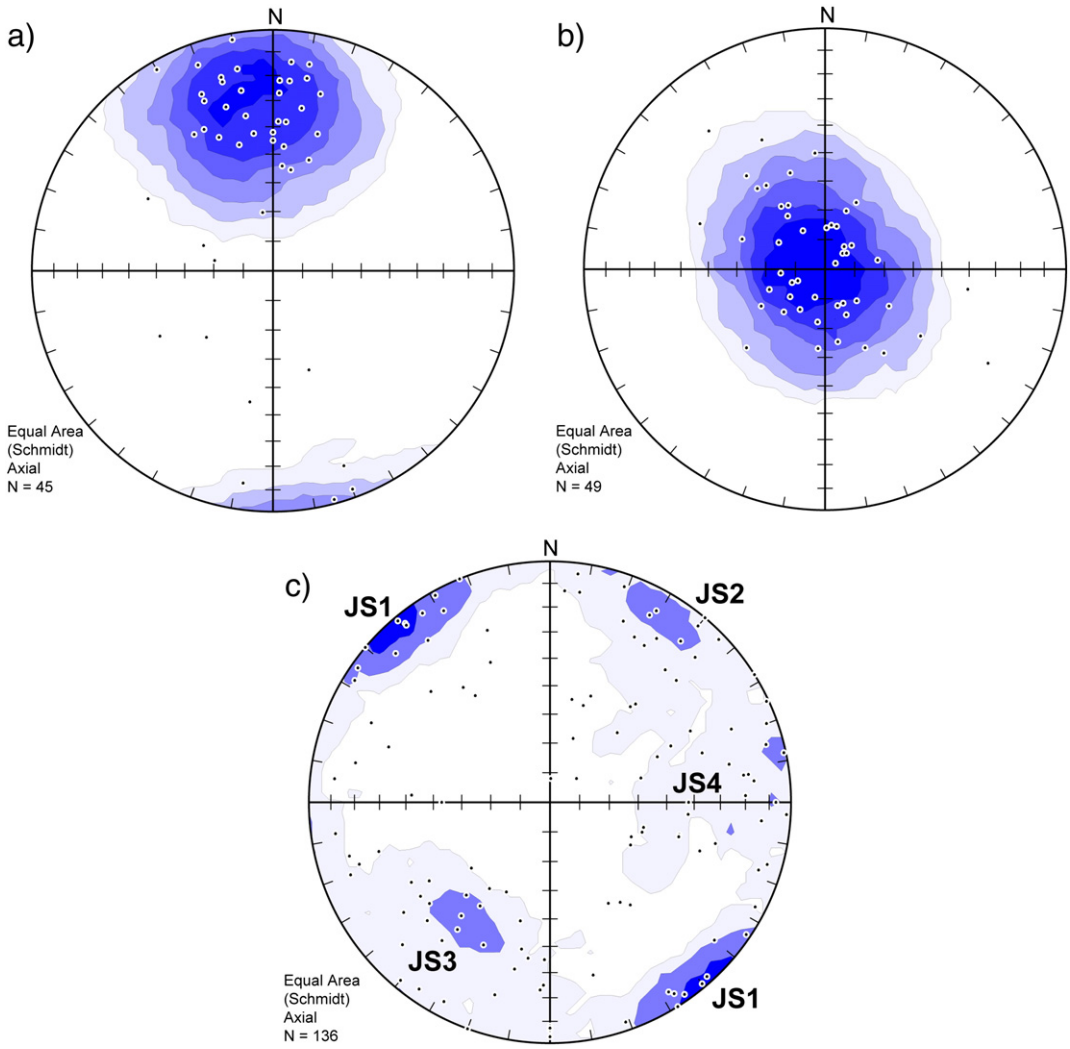

Fig. 4. Hemispherical projection of structural field data: Pole points of (a) foliation planes in the Landecker Quartzphyllite Zone, (b) foliation planes in the Silvretta Crystalline Complex, and (c) meso-scale fractures and their mean sets JS1 to JS4 within the Silvretta Crystalline Complex in the surroundings of the main scarp area (lower hemisphere).

by the Federal Office of Metrology and Surveying (BEV) as a trigonometrical survey whereby for several survey points the elevation was not determined. Therefore 11 survey points have been instrumented at the foot of the north-dipping slope whereby five survey points were installed inside the rockslide area (Point no. 131, 133, 138, 139, and 140, Fig. 1, Table 1). The four survey points no. 132, 134, 135 and 136, were placed at a currently dormant deep-seated rockslide which is located east from the Niedergallmigg rock slide. The two survey points 130 and 137, respectively, were installed outside of the rock slide.

The second geodetic campaign was performed in 1996 and the survey points were re-measured by means of GPS methods (Rittinger, 1997). During this campaign, mean annual velocities of more than 10 cm a^{-1} were observed. Furthermore it was found that the mean slope velocity varies on the surface of the slide. A continuous velocity decrease from 0.071 m a^{-1} to 0.035 m a^{-1} between the survey point no. 140 in the centre of the slide and the survey point no. 138 at the western flank of the slide was observed. Survey point no. 133, which is installed at the toe of the rock slide near the eastern boundary, shows very low displacement rates of 1 mm a^{-1} (Fig. 1). Because there are no surveying precision values available, it is questionable whether the slope is moving at extremely slow rates or whether it is actually dormant.

In the framework of a third and more detailed investigation program the Niedergallmigg rock slide was surveyed using tachymetric methods (Table 1). On Oct. 22, Nov. 12 and Nov. 17 2003, the pre-existing survey points and 20 additional ones were measured to determine their 3-D coordinates. In order to minimise air refraction influences on measurement accuracy, two-way surveys were done by using two total stations (i.e. at the same time one total station is positioned inside the slide and one at the stable fixed-point outside the slide). Follow-up surveys were performed in May 2004, April/May 2005 and November 2005. These results show that for the survey points no. 131, 138, 139 and 140 the mean annual velocity varied between 3.5 and 7.1 cm a^{-1}, within the time interval 2003 to 2005. The previously observed velocity increase towards the centre of the slide was confirmed during these campaigns (Fig. 8). New survey points installed higher up on the rock slide (i.e. 154, 155, 1551 and 159) show velocities between 7.1 and 7.8 cm a^{-1}. Given that these surveys determined the horizontal position and the altitude of the points, the mean dip angles of total displacement vectors were determined based on regression analyses. It was found that the dip angle of the displacement vectors increased from 6° at the toe to 36° in the upper part of the slope (Fig. 9). Again, for survey point no. 133 only a minor displacement rate in the range of a few mm's per year was observed which is within the accuracy of ± 2 cm of the survey run. Based on this, it is assumed that survey point no. 133 is actually not affected

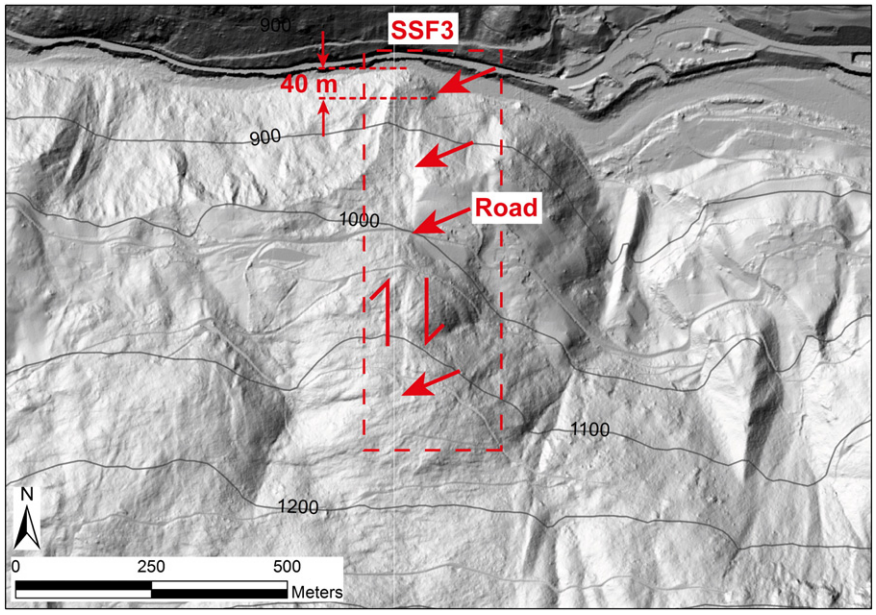

Fig. 5. Detail view of the northeastern part showing the strike-slip fault between the dormant and active part of the rock slide (for location see Fig. 1). Arrows indicate the morphologically defined surface trace of the dextral strike-slip fault (SSF3), the location where the sealed road is affected due to shearing by the slope movements (regular remedial maintenance is necessary), and the shear offset of about 40 m at the valley bottom.

by considerable slope deformations. It is therefore evident that between the two survey points no. 133 and 140, a discrete strike-slip shear zone exists which can be observed morphologically in the field (SSF3 in Figs. 1 and 5).

5. Geometrical model of the rock slide

Geological mapping, seismic investigations (Fig. 6) and deformation monitoring show that the Niedergallmigg rock slide has a maximum thickness of at least 300 m and a volume of 0.43 km^3. Geodetic deformation measurements indicate that the dip angle of total displacement vectors increases from 6° in the lower part to 36° in the upper part of the slope (Fig. 9). This and the shape of the basal sliding surface obtained from the seismic survey suggest that the slope kinematics is characterised by a rotational sliding behaviour along a basal shear zone (Fig. 10). The dip angle of the inferred basal shear zone varies between 5° and 45°. Unfortunately, the occurrence of a fully persistent basal shear zone has not been proven so far from data obtained from inclinometer boreholes. Nevertheless the development of a main scarp as well as distinct left and right flanks across the entire slope, the large shear offset in the main scarp face (i.e. more than 200 m in the Matekopf summit area) and the distinct seismic velocity contrast between the rock slide mass and the undeformed bedrock suggest that a coherent basal shear zone has developed. Furthermore, it is observed that simple back-rotation without internal deformation of the slide mass along the inferred basal shear zone does not result in the pre-failure slope topography. Zones of depletion and accumulation are formed on the one hand

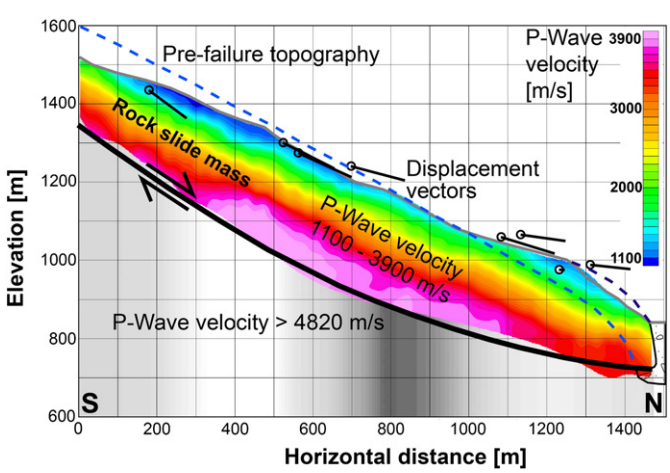

Fig. 6. N–S orientated seismic cross section (close to trace A–A′, see Fig. 1) showing the vertical P-wave velocity distribution and the inferred basal boundary of the rock slide. Below the basal shear zone the P-wave velocity is within the range of 4800 to 5400 m s^{-1} (grey shades).

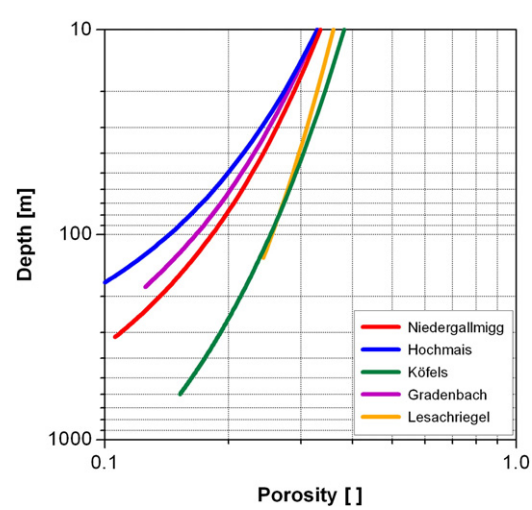

Fig. 7. Depth dependence of the in-situ rock mass porosity of several case studies based on the P-wave velocity (empirical correlation of Watkins et al., 1972).

Table 1
Geodetic deformation measurements depicting E–W (d*x*), N–S (d*y*), vertical (d*z*), horizontal (d*xy*) and total (d*xyz*) displacements in relationship to the reference survey from 2003 and the mean dip angle based on regression analysis.

Survey point number	Measuring date	E–W* [m] d*x* [m]	N–S* [m] d*y* [m]	Elevation [m] d*z* [m]	Horizontal displacement (d*xy*) in[m]	Total displacement (d*xyz*) [m]	Mean dip angle [°]
139	12.11.2003	21634.547	219328.176	987.642	0.000	0.000	6.31
139	18.05.2004	−0.013	0.030	0.008	0.033	0.034	
139	14.04.2005	0.007	0.071	0.000	0.071	0.071	
139	04.11.2005	−0.021	0.101	−0.010	0.103	0.104	
137	12.11.2003	21329.414	219030.428	1121.719	0.000	0.000	-
137	18.05.2004	0.008	0.000	0.010	0.008	0.013	
137	14.04.2005	0.019	−0.006	0.011	0.020	0.023	
137	04.11.2005	−0.006	0.004	−0.003	0.007	0.008	
138	22.10.2003	21467.070	219222.524	1044.012	0.000	0.000	8.96
138	18.05.2004	0.009	0.022	0.013	0.024	0.027	
138	14.04.2005	0.012	0.042	−0.002	0.044	0.044	
138	04.11.2005	0.011	0.070	−0.012	0.071	0.072	
131	12.11.2003	21717.217	219149.400	1064.786	0.000	0.000	8.03
131	18.05.2004	0.000	0.029	−0.007	0.029	0.030	
131	14.04.2005	0.004	0.075	−0.021	0.075	0.078	
131	04.11.2005	0.006	0.115	−0.014	0.115	0.116	
140	22.10.2003	22065.622	219098.606	1058.603	0.000	0.000	17.02
140	18.05.2004	0.016	0.039	−0.001	0.042	0.042	
140	14.04.2005	0.009	0.106	−0.023	0.106	0.109	
140	06.11.2005	0.004	0.138	−0.042	0.138	0.144	
133	17.11.2003	22705.998	219247.754	974.596	0.000	0.000	-
133	18.05.2004	−0.012	0.013	0.005	0.018	0.018	
133	15.04.2005	0.004	−0.017	0.006	0.017	0.018	
133	05.11.2005	−0.008	0.007	0.011	0.011	0.015	
154	22.10.2003	21877.482	218713.016	1240.343	0.000	0.000	14.82
154	12.05.2004	0.001	0.035	−0.017	0.035	0.039	
154	10.05.2005	−0.013	0.101	−0.039	0.102	0.109	
154	06.11.2005	−0.011	0.139	−0.035	0.139	0.144	
155	22.10.2003	22211.173	218578.643	1273.892	0.000	0.000	24.40
155	12.05.2004	−0.008	0.042	−0.013	0.043	0.045	
155	10.05.2005	−0.009	0.103	−0.051	0.103	0.115	
155	06.11.2005	−0.018	0.137	−0.058	0.138	0.150	
1551	22.10.2003	22219.754	218538.394	1300.319	0.000	0.000	26.71
1551	12.05.2004	−0.002	0.041	−0.008	0.041	0.042	
1551	10.05.2005	0.002	0.097	−0.050	0.097	0.109	
1551	06.11.2005	−0.012	0.134	−0.062	0.135	0.148	
159	22.10.2003	22056.355	218193.744	1434.82	0.000	0.000	36.41
159	12.05.2004	−0.004	0.035	−0.003	0.035	0.035	
159	11.05.2005	−0.002	0.099	−0.069	0.099	0.121	
156	22.10.2003	22929.907	218584.444	1282.628	0.000	0.000	-
156	12.05.2004	0.017	0.009	0.011	0.019	0.022	
156	10.05.2005	0.006	−0.002	0.019	0.006	0.020	
156	06.11.2005	0.004	0.009	0.035	0.010	0.036	

* Gaus-Krüger Coordinates of reference survey 2003.

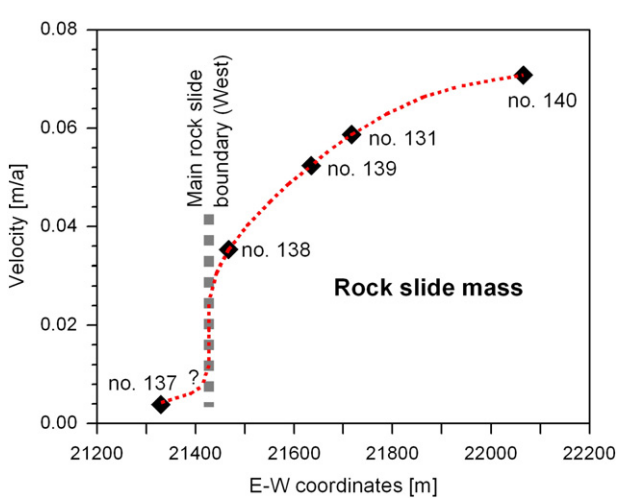

Fig. 8. Spatial distribution of the slope velocity across the northwestern boundary near the Niedergallmigg Village (location of survey points are shown in Fig. 1).

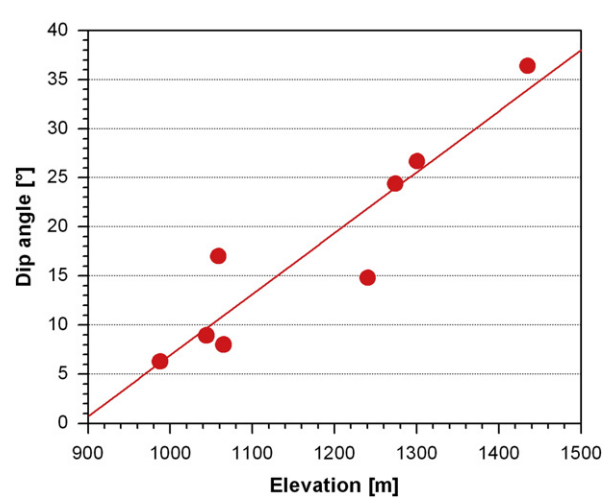

Fig. 9. Dip angle of the total displacement vectors versus elevation suggesting a rotational character of the slide.

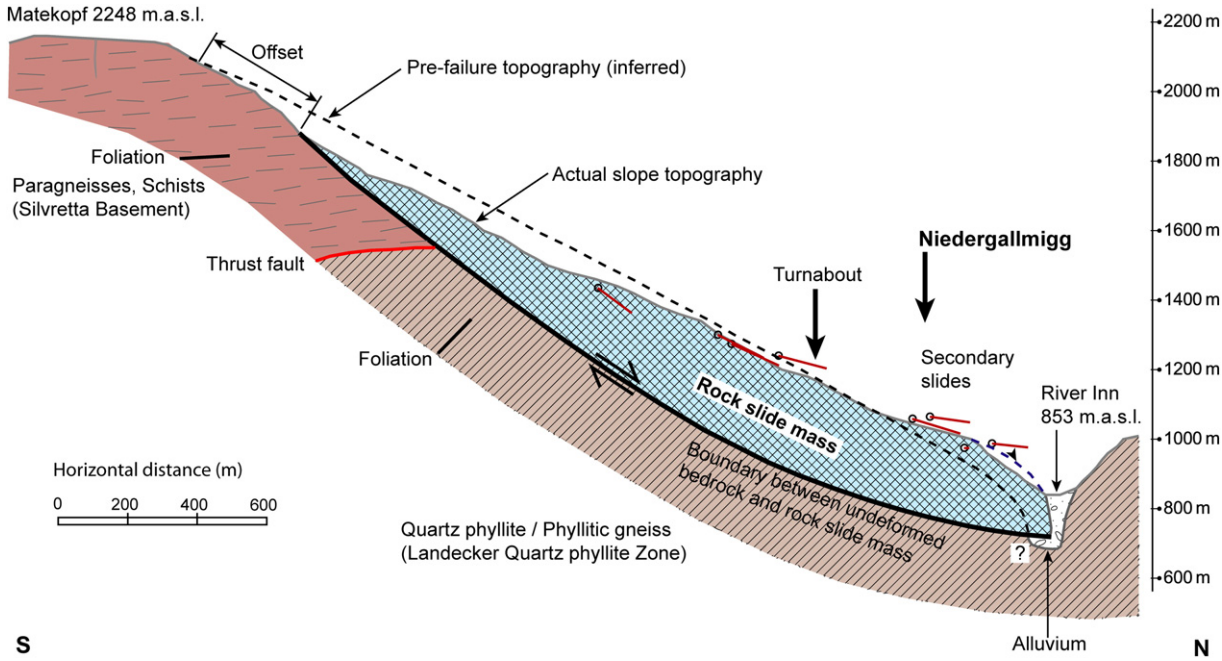

Fig. 10. N–S cross section along A–A′ (for location see Fig. 1) showing the rock slide geometry, actual and pre-failure topography, geological setting, and dip of total displacement vectors of geodetic survey points.

due to mass relocation and on the other hand due to internal rock mass deformation.

The ongoing slope movement towards north caused compression of and/or thrusting on the alluvium at the toe of the slope (Figs. 1 and 5). The course of the River Inn has been deflected and pushed towards north. At the western flank near the valley bottom (i.e. the strike-slip fault SSF1), the rock slide offset exceeds more than 120 m. Similar observations were made on the eastern head flank of the rock slide (i.e. the strike-slip fault SSF2), where the River Inn has been considerably deflected from its original course. The dextral strike-slip fault SSF3 has split the rock slide body into two slabs: a western one which is active and an eastern one, which is most likely dormant (Fig. 5). Further, in the valley floor a dextral slip offset of about 40 m was measured along the fault SSF3. This led to compression of the alluvium in front of the western slide mass. The eastern part of the rock slide system i.e. the slab between the strike slip faults SSF2 and SSF3 is either inactive/dormant or only marginally active of a few mm per year. This is contrary to the western sliding slab i.e. between SSF1 and SSF3 where increasing velocities towards the centre of the slide were measured within the time interval 2003 to 2005 (i.e. from 3.5 to 7.1 cm a^{-1}).

As mentioned above, the distance between the upper main scarp and the upper boundary of the sliding mass indicates a total displacement of more the 200 m. A main geomorphological feature of the Niedergallmigg rock slide, but also of numerous other case studies in mica-rich crystalline rock masses is the enormous failure/displacement induced topographical change relative to the pre-failure slope topography. On the one hand, the middle to upper area of the rock slide is characterised by considerable surface subsidence and mass losses. On the other hand, the foot of the slope features bulge-like slope geometries and rock mass accumulation. Furthermore the advancing slope deformation process and river erosion causes an oversteepening of the foot slope. In Niedergallmigg the turnabout between mass loss (settlement) and mass accumulation areas was found at an elevation between 1000 and 1100 m a.s.l. Thus the newly formed slope geometry is the product of failure and sliding-induced internal strains, and fracturing and the fragmentation of the rock mass. The reduced strength of the rock mass and slope toe oversteepening lead to first-time, small-scale secondary rock slides (Fig. 1). In the following section, a quantitative volume/mass balance calculation between pre-failure and actual topographies is given.

6. Rockslide volume/mass balance estimations

The north-facing Niedergallmigg rock slide is characterised by an exceptionally well-featured main scarp and right as well as left flanks. This enables a reliable pre-failure topography reconstruction by modifying topographical elevation lines between the right and left flanks. A first approach focuses on a section area balance i.e. area loss and area increase along the cross section A–A′ (Figs. 1 and 10). A second approach is based on volume balancing (i.e. elevation difference models) between the actual and the pre-failure slope topography by means of GIS (Geographical Information Systems). In order to reconstruct the pre-failure topography, a one metre raster digital terrain model obtained through airborne laser scanning was used. Elevation lines of the actual rock slide mass were reshaped to fill up the depletion zone or to remove the accumulation zone based on the slope geometry of the left and right flanks. After reconstruction area/volume balancing between the pre- and post-failure slope was made. Rock mass area/volume loss in the depletion zone was compared with area/volume increase in the accumulation zone of the slide.

Results from the first method show that along cross section A–A′ the cross section area was reduced by 92,000 m^2 for the upper and middle areas of the slide (Figs. 1 and 10). In contrast an area increase of only 36,000 m^2 was obtained in lower areas. Thus a ratio of 2.6 is obtained between area reduction and increase.

The GIS-based volume balance analyses between the upper and middle parts, respectively, and the lower part show similar trends. The volume loss (i.e. surface subsidence) area gains more than 85 million m^3. In the lower part a rock mass volume increase of only 30 million m^3 was obtained. This yields into a ratio of 2.8 which agrees with estimations from the area-based method. If deformation-induced dilatation effects (i.e. mean porosity increase to 17%) of the rock mass are additionally

considered, then the volume imbalance is even larger. These mass balance analyses suggest that the rock slide experienced considerable rock mass volume loss of more than 55 million m^3 in its history.

Failure volume estimations of smaller scale secondary slides at the toe of slope show slide volumes of only a few million m^3. Thus these volumes are a magnitude lower than the total volume loss which suggests that rock mass degradation could result from several secondary rock slide events and/or continuous erosion processes at the foot of the slide (i.e. polyphase events). This hypothesis was confirmed during recently observed slope foot erosion processes during flooding events (e.g. summer 1954) when numerous secondary slides were triggered.

7. Numerical modelling

In order to study the influence of the alluvium at the foot of the slope on the deformation characteristics, several 2-D numerical models were constructed by means of the Universal Distinct Element Code UDEC (Itasca, 2007). In other words, the impact of the alluvium acting as a buttress mass at the foot on stability and displacement of the slope was investigated. Generally, this software has the capacity to simulate large deformations and block interactions. Therefore strength properties of the basal shear zone are varied and total shear displacements are numerically calculated. In the case where the basal shear zone is set to shear strength properties at or below limit-equilibrium conditions, slope displacement initiates and is ongoing as long as a stable configuration and numerical equilibrium is reached. This means that under ongoing displacements a safety factor cannot be determined reliably. In order to avoid safety factor calculations, this study focusses on shear displacements at the basal shear zone and its relationship to assigned shear strength properties. In doing so, the transition from minor i.e. predominately elastic slope conditions to large slope displacements can be determined as a friction angle–displacement relationship. Model runs considering both alluvium and no alluvium were performed. Conceptually, removing the alluvium at the foot of the slope change the in-situ stress conditions of the rock slide system and thus reduce slope stability considerably. The difference of friction angles between the alluvium and no alluvium model geometries represents a measure of the buttressing effect.

Furthermore, back-calculations focusing on the in-situ shear strength parameters (i.e. friction angle) of the basal shear zone were done. Based on water-free and saturated groundwater models back-calculated shear strength values were compared with laboratory results from shear zone specimens composed of fault gouges and breccias sampled in similar geological conditions.

7.1. Numerical model geometry, mechanical and hydraulical parameters and boundary conditions

A two-dimensional numerical model geometry considering the main features of the geological cross section was constructed (Fig. 11). Based on the results from the seismic investigations and geodetic surveys, a basal shear zone was incorporated in terms of several straight-line contact segments. In addition, continuous horizontal and vertical discontinuities were included. The main reason to include these discontinuities was that the model should be able to consider hydraulic fluid flow. Although the orientation of the discontinuities does not coincide with the field measurements, the implemented fracture pattern enables us to define horizontal and vertical hydraulic conductivity values. For each model unit i.e. the bedrock, the rock slide and the alluvium discontinuity spacing and aperture are set equally in order to maintain isotropic hydraulic conditions. The discontinuity pattern assigned to alluvial deposits does not reflect geological in-situ conditions, but this is related to the limitation of the software UDEC which can consider fluid flow only along discrete discontinuities by means of the cubic law. Porous fluid flow which usually takes place in an alluvium or a soil cannot be modelled. Nevertheless this hydrogeological disadvantage of the software UDEC is compensated by its great capacity to model and study the mechanical behaviour of block interactions and large shear displacements along discontinuities, which is a major focus of this study. The fracture sets and the basal shear zone enables considerable internal rock mass deformation in a tensile and shear mode.

According to the mechanical block behaviour within the bedrock and sliding mass unit, linear-elastic constitutive relationships are assigned. In contrast, alluvial sediments are characterized by elasto-plastic material models. According to the implementation of contact laws in UDEC all discontinuities are characterized by a Coulomb slip model (Table 2, Itasca, 2007).

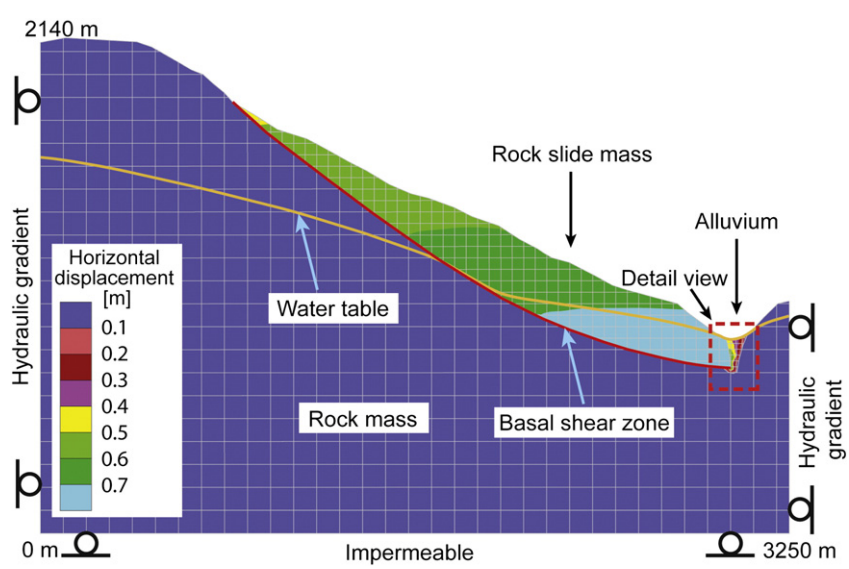

Fig. 11. 2D geometrical model and boundary conditions of the rock slide for numerical analyses based on the geological cross section in Fig. 10. Model set up considering alluvial deposits and steady state groundwater flow. Horizontal displacement contours in metres of the rock slide mass, the location of the detail view (Fig. 13), and the numerically determined water table are shown.

Table 2
Material properties of paragneissic rock mass for the failure initiation and sliding model.

	Parameter	Value
Bedrock	Density [kg m^{-3}]	2600
	Bulk modulus [GPa]	20
	Shear modulus [GPa]	9
Rock slide	Density [kg m^{-3}]	2600
	Bulk modulus [GPa]	17
	Shear modulus [GPa]	8
Alluvium	Density [kg m^{-3}]	2000
	Bulk modulus [GPa]	0.2
	Shear modulus [GPa]	0.05
	Cohesion [MPa]	300
	Friction angle [deg]	30
Basal shear zone	Normal stiffness [MPa mm^{-1}]	100
	Shear stiffness [MPa mm^{-1}]	100
	Cohesion [MPa]	0
	Friction angle [deg]	varied
	Apertures (azero/ares) [mm]	0.5 / 0.5
	Joint permeability factor [Pa^{-1} s^{-1}]	83.3
Joints	Spacing bedrock [m]	100
	Spacing rock slide [m]	50
	Spacing alluvium [m]	25
	Normal stiffness [MPa mm^{-1}]	100
	Shear stiffness [MPa mm^{-1}]	100
	Cohesion [MPa]	0
	Friction angle [deg]	40
	Apertures (azero/ares) [mm]	0.25/0.25
	Joint permeability factor [Pa^{-1} s^{-1}]	83.3

*Varied to induce failure.

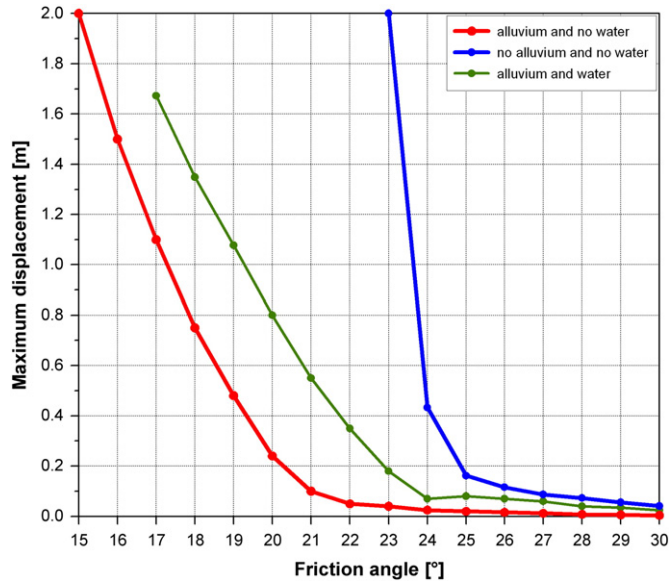

Fig. 12. Relationship between maximum shear displacement at the basal shear zone and the implemented friction angle: (a) Model set up considering alluvial sediments but no groundwater, (b) model set up characterised by no alluvial sediments and no groundwater, and (c) model set up with alluvial deposits and steady state groundwater flow (shear strength back-calculation).

Generally, the hydrogeological situation is sparsely defined. Referring to the experience of other case studies of rock slides in metamorphic rocks, a conceptual hydrogeological model comprising of a higher permeable rock slide mass, a lower permeable bedrock below and a highly permeable shear zone in between was designed (Bonzanigo et al., 2007; Loew and Strauhal, 2013, 2014; Zangerl et al., 2013). Geophysical investigations gave porosities of rock slide masses in the range between 11% and 33%. Given that such high porosities resulted from extensive internal rock mass fracturing and cataclasis, it is assumed that a hydraulically conductive fracture/pore network enables adequate fluid flow. Hydraulic packer tests confirm these conceptual considerations and show an extremely large bandwidth and a heterogeneous spatial distribution of hydraulic conductivity values for rock slide masses in the range between 1×10^{-2} and 1×10^{-7} m s^{-1} (Bonzanigo et al., 2007; Zangerl et al., 2013). A higher rock slide permeability relative to the bedrock would cause a low and flat lying water table in the rock slide mass. Ongoing mechanical fracturing and cataclasis of the rock slide mass causes uncemented fault gouges and breccias at the basal shear zone. If there are only thin clayey-silty fault gouge layers, the basal shear zone show a high hydraulic conductivity. But if a thick and persistent fault gouge layer is formed within the basal shear zone, a hydraulic barrier with a considerable reduced permeability may affect the groundwater flow field. In this study it is assumed that the impact of low-permeable fault gouges can be neglected and the basal shear zone is composed of high-permeable fracture zones and fault breccias. Concerning fracture spacings and apertures shown in Table 2 hydraulic conductivities of 2.6×10^{-7} m s^{-1} for the sliding mass, 1.2×10^{-7} m s^{-1} for the bedrock and 5.1×10^{-7} m s^{-1} for the alluvial sediments were chosen. Hydraulic boundary conditions for the left and right model boundaries were defined as fixed fluid pressure with a vertical gradient (Fig. 11). The lower hydraulic model boundary was set to be impermeable. The left, right and lower mechanical model boundaries were assigned as roller boundaries.

7.2. Influence of alluvial sediments on slope deformation

Given that the foot of the rock slide is covered by thick alluvium, the stabilisation effect of these sediments was studied in detail by using numerical modelling. The friction angle of the basal shear zone was varied by intervals of one degree and the resulting shear displacements of the overall rock slide mass were numerically monitored. In order to guarantee that the model parameters, the stress state and the boundary conditions remain constant within similar model runs, simulations were performed without groundwater flow. To study the impact of the alluvium on slope displacement, two model types were built: one considering alluvium at the foot of the slope ("alluvium model") and the other without it ("no alluvium model"). The results of these models were then compared to each other (Fig. 12).

The results show that the stresses from the alluvium acting at the foot considerably affect the slope deformation behaviour. Maximum slope displacements of less than 0.16 m and slope stabilisation is reached for the "no alluvium model" when a friction angle larger than 25° was considered (Fig. 12). In contrast, model runs considering alluvium at the foot of the slope achieved slope stabilisation at a much lower friction angle of about 21°. There is no sharp boundary but rather a transition zone between stable and unstable model conditions. The difference of about 4° of the friction angle between these two model types is preeminent (Fig. 12). Furthermore the alluvium has a considerable impact on the shape of the friction angle versus displacement curve. Without alluvium at the foot of the slope the friction angle versus displacement curve increases steeply within a small friction angle bandwidth of less than 2°. The transition from stable to unstable slope conditions is sharp. In contrast, the slope of the friction angle versus displacement curve obtained from calculations with alluvium is gently increasing over a much wider range of friction angles of 9°. For comparison of both model types a maximum displacement value of 2 m was chosen. The modelling result suggests that rapid failure would be prevented even if the frictional strength along the basal shear zone is reduced considerably. This mechanism can avoid slope acceleration to dangerous velocities because an abrupt reduction of the overall slope strength does not occur. In other words the alluvium can stabilise the slope and reduce the "brittleness" of the rock slide system.

In the models series rock slide deformation accumulates primarily along the basal shear zone without relevant internal deformation of the rock mass indicating en bloc movement. Shear displacement along

the basal shear zone increases from the main scarp to the foot of the rock slide by less than 25%. Internal strains of the blocks and shear displacements along horizontal and vertical discontinuities in the rock slide are small. Shear displacement and opening are generally smaller than a few millimetres.

Plasticity and displacement plots indicate that the alluvium experiences shear and tension failures, compaction and uplift (Fig. 13). So far it is unclear if the modelled uplift in the range of several decimetres to metres is related to real in-situ conditions or to model artefacts induced by the model setup. Generally, two-dimensional plane strain models do not consider out of plane displacements. Conceptually, compaction of the alluvium may lead to both a reduction of porosity and uplift. Unfortunately, geodetic levelling measurements were not performed across the valley bottom which would enable the validation of the numerically simulated uplift deformation.

7.3. Back-calculation of shear strength properties of the basal shear zone

Additional model analysis was performed to back-calculate the friction angle of the basal shear zone. Based on the assumption that the basal shear zone in Niedergallmigg primarily consists of uncemented fault gouges and breccias (kakirites), it is assumed that cohesion is very low if not close to zero. Numerous laboratory tests e.g. based on ring shear testing methods show that low cohesion values (<20 kPa) for kakirites are frequently observed (Strauhal, 2009).

In contrast to the modelling campaigns in Section 7.2, this series of modelling included stationary groundwater flow. Due to the lack of comprehensive in-situ groundwater investigations (e.g. piezometers), the spatial distribution of the initial groundwater level is estimated and the input data for the model was based purely on conceptual considerations. Furthermore, hydraulic conductivity values for the undeformed bedrock, the rock slide mass and the basal shear zone are taken from literature (Loew and Strauhal, 2013, 2014; Zangerl et al., 2013). Although the absolute values are fraught with high uncertainties, properly assigned conductivity differences may help to provide some useful indications of the pore pressure distribution. The contrast in hydraulic conductivity between the rock slide mass and the bedrock with highly permeable basal shear zone induces a steady state pore pressure distribution characterised by a more steeply inclined water table (approx. mean of 25°) in the bedrock than along the basal shear zone, and a more gently inclined gradient (approx. mean of 11°) in the higher permeable rock slide (Fig. 11). In contrast to the fractured bedrock, the twice higher permeable rock slide mass lead to a lower and less inclined groundwater table.

Back-calculation based model runs showed that a friction angle of about 24° and cohesion of 0 MPa produced the most feasible model results (Figs. 11 and 12). The impact of groundwater flow on slope stability is relevant and a 2–3° higher friction angle is required to gain stability than under water-free conditions.

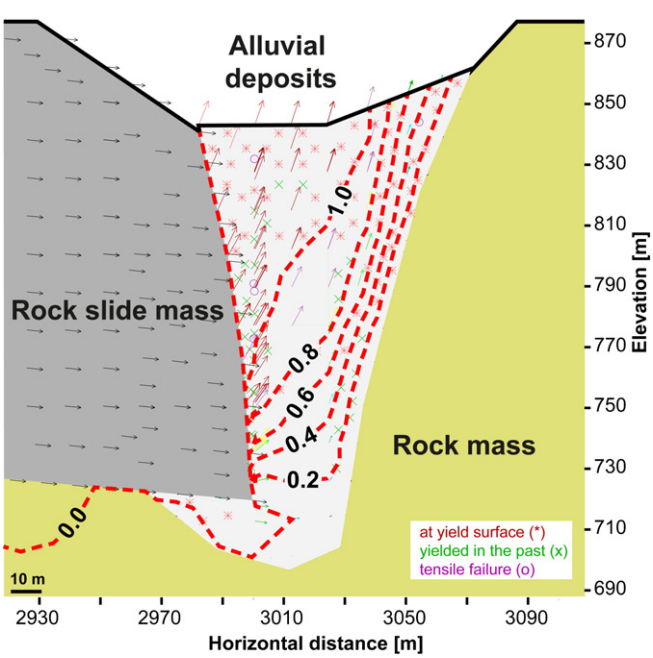

Fig. 13. Detail view focussing on the alluvial sediments. Vertical displacement contours in metres (uplift), displacement vectors and plasticity indicators provide some insight of the deformation characteristics of alluvial sediments at the toe due to compression by the slide.

8. Discussion

8.1. Conceptual deformation model

The structural inventory suggests that large-scale flexural toppling was a primary deformation mechanism during the initial formation stage of the rock slide (Figs. 1 and 14a). Steeply inclined E–W striking brittle fault zones as well as foliation planes dipping into the slope generate a rock mass anisotropy which is prone to toppling. Toppling along these discontinuities causes morphological features such as graben structures over the entire slope i.e. inside and outside of the rock slide mass (Fig. 1). The lack of representative rock outcrops within the slide mass and the large variation of dip angles of foliation planes make it difficult to quantify the amount of toppling, i.e. the tilting of foliation and fault planes before and after the toppling process. So far we assume that toppling of the rock mass did not reach the large magnitudes which were observed for example in La Clapiere, where the tilting angle is in the range of 40° (Guglielmia et al., 2000). In addition, the formation of the lateral boundary of the rock slide mass is structurally controlled by the joint sets JS1, JS3, and JS4. The discrepancy between the pre-failure topography and the rock slide geometry as well as the high degree of rock mass fragmentation indicate that considerable internal strains have occurred in the rock slide mass. Furthermore, simple en block back movement without internal rock mass deformation does not lead easily to the pre-failure slope geometry. Initial slope toppling processes may have induced internal rock mass strain, in-plane shearing, fracturing and dilatation to great depth (Fig. 14b). As a hypothesis these mechanical processes weaken the overall strength of the rock mass. The pre-failure topography changes continuously with the upper part of the slide experiencing subsidence and the lower part bulging. At a later stage, when slope deformation further developed, strain localization increasingly became the dominant process and finally a continuous basal shear zone was progressively formed (Fig. 14c). Depending on the kinematics and deformation processes internal shear zones within the rock slide mass were also formed. Finally, slope deformation accumulates predominately along shear zones and internal rock mass deformation becomes a secondary process. The results of the field observations and geodetic surveys as well as the seismic data suggest that a basal shear zone has developed.

Due to the lack of inclinometers in this study, it could not be proven if the currently measured surface deformation results solely from shearing along the basal shear zone or from both the shear zone and internal rock mass deformation. Tachymetric surveys on the lower part of the slide show movement rates that increase from the left flank to the centre (Fig. 8). This suggests that laterally internal rock mass deformation is still ongoing and differential movements are occurring. Slope velocities obtained from the geodetic surveys between 2003 and 2005 point to an increase from the main scarp (survey point no. 138) to the centre by a factor of two (survey point no. 140). The occurrence of considerably differential movement rates in this region of the slide is further confirmed by the extensive cracking of brick walls on several buildings located near the left flank of the slide. Shear strain

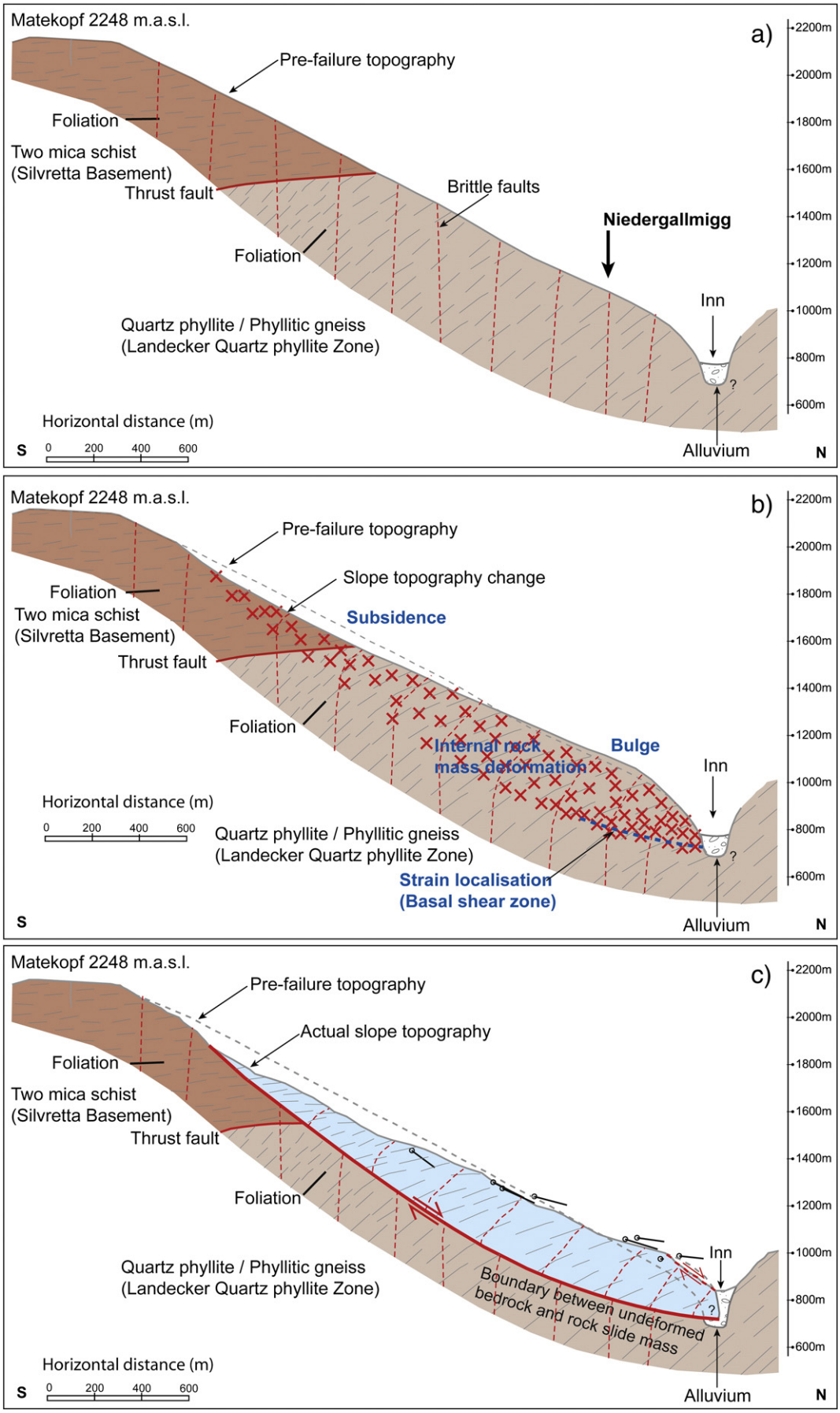
Matekopf 2248 m.a.s.l.
a)
Pre-failure topography
Foliation
Two mica schist
(Silvretta Basement)
Thrust fault
Brittle faults
Niedergallmigg
Foliation
Inn
Quartz phyllite / Phyllitic gneiss
(Landecker Quartz phyllite Zone)
Horizontal distance (m)
S
0 200 400 600
Alluvium
N
2200m
2000m
1800m
1600m
1400m
1200m
1000m
800m
600m
Matekopf 2248 m.a.s.l.
b)
Pre-failure topography
Slope topography change
Foliation
Subsidence
Two mica schist
(Silvretta Basement)
Thrust fault
Foliation
Internal rock
mass deformation
Bulge
Inn
Horizontal distance (m)
0 200 400 600
Quartz phyllite / Phyllitic gneiss
(Landecker Quartz phyllite Zone)
Strain localisation
(Basal shear zone)
S
Alluvium
N
Matekopf 2248 m.a.s.l.
c)
Pre-failure topography
Actual slope topography
Foliation
Two mica schist
(Silvretta Basement)
Thrust fault
Foliation
Inn
Quartz phyllite / Phyllitic gneiss
(Landecker Quartz phyllite Zone)
Boundary between undeformed
bedrock and rock slide mass
Horizontal distance (m)
S
0 200 400 600
Alluvium
N

inside the rock mass yields 6×10^{-5} m m^{-1} per year (survey points no. 138 and 140) and across the main scarp it is at least larger than 2×10^{-4} m m^{-1} per year (survey points no. 137 and 138), respectively.

Deformation surveys on the Niedergallmigg rock slide show that a slab located in the lower part near the right flank at the eastern boundary is currently stable and that the boundary to the western active rock slide mass is a steeply inclined dextral strike-slip fault. The mechanical interaction of this rock slide slab with the alluvium at the foot of the slope may have caused the observed stabilisation.

The large displacements of the Niedergallmigg rock slide changed the pre-failure slope topography and rock slide geometry considerably and induced internal rock mass strains. This affected the mechanical and hydrogeological rock mass properties as well as the in-situ stress conditions especially at the toe due to slope oversteepening. As a consequence of the reduced rock mass strength and the newly formed slope geometry, secondary rock slides have developed.

Furthermore, it is assumed that slope erosion at the foot of the slope by the River Inn and heavy rainfall as well as snowmelt additionally helped the formation of these secondary slides. Volume balance analyses showed that at the foot a rock slide volume of more than 55 million m^3 is missing. The appearance of secondary slides and the deflection of the course of the River Inn suggest that fluvial erosion processes led to such losses of mass. The complex interaction between geometrical changes and strength reduction of rock slides, the formation of secondary failure events at the foot of the slope and river erosion may play an important role in keeping deep-seated rock slides active. A comparison with measured annual erosion/transport capacities of rivers in alpine catchment areas (Tschada and Hofer, 1990) suggest that the volume loss of the Niedergallmigg rock slide can be easily reached during a time span of several hundred years. Furthermore abnormal precipitation and following flood events may even increase the erosion capacity of the River Inn.

8.2. Influence of alluvium

The influence of alluvium at the foot of the slope on the slope stability is considerable and should be considered during slope stability and deformation calculations. Generally, the alluvium has a relevant stabilisation effect due to buttressing at the foot of the slope. The mechanical i.e. plastic soil behaviour of the alluvium leads to a less stiffer overall system behaviour, and the transition from stable to unstable behaviour is gradual. Given that the sedimentology and mechanical properties of the alluvium are extremely inhomogeneous (clay to bolder grain size), the models presented herein provide only some conceptual mechanisms of the system behaviour. Thus absolute values should be handled with caution and require a critical appraisal, because no in-situ investigations such as drillings as well as seismics and geodetic surveys were made along the foot of the slope. Based on field investigations along the valley bottom outside the study area, the alluvium consists of a complex and heterogeneous sequence of clay to boulder sized sediments. The thickness of the alluvium has not been explored in detail and thus its geometry is uncertain. It is possible that some parts of the rock slide i.e. especially the dormant slab east of the strike slip fault, are in contact with the bedrock on the opposite slope of the valley. The central and western part of the rock slide, which shows movement rates of up to 7 cm a^{-1} may not be in contact with the opposite valley flank even though the gap between them is only 20 to 40 m.

8.3. Shear strength properties of the basal shear zone

The observed offset in the main scarp area of more than 200 m and the long-term deformation history of the rock slide suggest that the basal shear zone is at or close to residual shear strength conditions (Skempton, 1964, 1985). Hence cohesion along the basal shear zone, subject to continual shearing, would be very low. The back-calculated friction angle indicates an overall shear strength at which shear displacement along the basal shear zone starts to accumulate. It may represent the frictional resistance which act actually and after a complex und unknown history of slope movement.

Back-calculations based on the linear Mohr-Coulomb strength criteria revealed an overall residual friction angle of 24° for the actual basal shear zone in the 2D Niedergallmigg rock slide model. For comparison, analyses of published case studies in similar metamorphic rock masses (i.e. phyllites, schists and gneisses) show a large range of shear strength values. All the case studies are characterized by a basal shear zone composed of uncemented fault breccias and gouges whereby some show additional internal shear zones which dominate slope kinematics and stability. According to the study of Zangerl et al. (2015), shear zones are extremely heterogeneous concerning grain size distribution, fracture density, shear zone thickness, roughness and waviness of the boundary to the less fractured bedrock. The occurrence of heavily fractured rock rafts embedded in a fine grained gouge/breccia matrix are observed.

Zangerl and Prager (2008) back-calculated a residual friction angle of 26° to 30° for a 50 m thick deep-seated rock slide in paragneissic rock. Based on the universal discrete element method, Eberhardt et al. (2007) obtained a basal shear zone friction angle of 34° for the deep-seated Campo Vallemaggia Landslide. The same rock slide calculated by the force-balance limit-equilibrium approach resulted in a friction angle of 31° and a cohesion of 100 kPa (Bonzanigo et al., 2007). Barla (2010) determined an in-situ friction angle of only 22° for a deep-seated rock slide close to the Beauregard Dam in Italy. Back-calculations based on a continuum approach focusing on the initial failure process show that for the rock slide Köfels a friction angle between 20° and 24° is required to trigger slope failure (Brückl and Parotidis, 2001). In comparison, ring shear tests performed on fault breccias and gouges (kakirites) produce residual strength values of 23° to 27° (Strauhal, 2009). Glastonbury and Fell (2008) analysed several slowly moving deep-seated rock slides in metamorphic rock. They compiled laboratory-derived residual friction angle data of basal shear zone material and obtained values between 18° and 27°.

Key sources of uncertainty are the geometry of the model, hydrogeological properties and boundary conditions, i.e., the pore pressure distribution. The obtained friction angle can vary in the order of a few degrees. In addition, the simplification of the natural rock slide geometry as a 2D numerical model lead to a neglecting of lateral boundary effects which can cause an underestimation of the friction angle (Skempton, 1985; Stark and Eid, 1998). Translational or rotational kinematics, sliding mass interactions and the interplay of alluvium at the toe of the slope with the rock slide further increase complexity of back-calculations and thus make comparison of different case studies difficult. Laboratory tests have several limitations which lead to difficulties when the results were directly compared with those from back-calculations. In particular, it is hardly possible to transfer the in-situ structural fabric of the shear zone and of pre-existing shear fractures (slickensides) into the laboratory. Furthermore, because the in-situ basal shear zone has a size which is many times larger than the shear

Fig. 14. Conceptual model of the rock slide system. (a) Toppling along foliation planes and steeply inclined E–W striking brittle fault zones. (b) Rock mass cataclasis, fragmentation, dilatation, subsidence and bulging, and initiation of strain localisation. (c) Development of a basal shear zone during a late stage of the formation process and ongoing sliding processes.

zone material tested in laboratory, the relevant time period between in-situ und laboratory differs enormously, and often the large bandwidth as well as distribution of in situ stresses cannot be adequately considered during testing campaigns.

9. Conclusion

Field surveys suggest that the primary slope deformation process during the initial formation stage of the Niedergallmigg rock slide was flexural toppling. Later on and presently slope deformation is due to rotational sliding along a basal shear zone at a depth of at least 300 m. It is concluded that the measured slope displacement predominantly accumulates along this basal shear zone. Nevertheless geodetic measurements at the surface indicate that some continuous internal rock mass deformations between the main scarp and the central part of the slide are still occurring.

Mass balance calculations, considering pre-failure and post-failure slope topographies, suggest that about 85 million m^3 of debris has been eroded by the River Inn. Secondary slope affecting processes such as slides and river erosion at the foot, most likely triggered by intensive rainfall periods and flooding events, were identified. They play a major role in the long-term development and activity history of slowly moving deep-seated rock slides.

Numerical modelling results based on the Universal Discrete Element Code (UDEC) showed a large influence on slope stability when the alluvium at the toe interacts with the rock slide. It could be proven that these sediments reduce the "brittleness" of the system i.e. the transition between small and large displacements is rather gradual than abrupt. Back-calculations based on model geometries considering both the existence of alluvium and the non-existence of alluvium show a friction-angle difference of about 4°. Back-calculations using the most plausible model set-up yields a friction angle of about 24°.

Acknowledgments

The authors wish to acknowledge and thank alpS GmbH, Tiroler Wasserkraft AG, ILF Consulting Engineers, geo.zt GmbH, and the Austrian Research Promotion Agency (COMET-program) for supporting this work.

References

Agliardi, F., Zanchi, A., Crosta, G.B., 2009. Tectonic vs. gravitational morphostructures in the central Eastern Alps (Italy): Constraints on the recent evolution of the mountain range. Tectonophysics 474, 250–270.
Agliardi, F., Crosta, G.B., Frattini, P., 2012. Slow rock-slope deformation. In: Clague, J.J., Stead, D. (Eds.), Landslides: Types, mechanisms and modelling. Cambridge University Press, pp. 207–221.
Amann, F., 2006. Großhangbewegung Cuolm da Vi (Graubünden, Schweiz). Geologisch-geotechnische Befunde und numerische Untersuchungen zur Klärung des Phänomens. Dissertation thesis. Friedrich-Alexander Universität Erlangen-Nürnberg, Deutschland.
Barla, G., 2010. Long term behaviour of the Beauregard dam (Italy) and its interaction with a deep-seated gravitational slope deformation. In: Tentschert, E., Poisel, R. (Eds.), 5th colloquium rock mechanics – Theory and practice. Mitteilungen für Ingenieurgeologie und Geomechanik 9, pp. 111–125.
Bonzanigo, L., Eberhardt, E., Loew, S., 2007. Long-term investigation of a deep-seated creeping landslide in crystalline rock – Part 1: geological and hydromechanical factors controlling the Campo Vallemaggia landslide. Can. Geotech. J. 44, 1157–1180.
Brandner, R., 1980. Geologische und Tektonische Übersichtskarte von Tirol, Tirol-Atlas. Univ.-Verlag Wagner, Innsbruck.
Brückl, E., Parotidis, M., 2001. Estimation of large-scale mechanical properties of a large landslide on the basis of seismic results. Int. J. Rock Mech. Min. Sci. 38, 877–883.
Brückl, E., Parotidis, M., 2005. Prediction of slope instabilities due to deep-seated gravitational creep. Nat. Hazards Earth Syst. Sci. 5, 155–172.
Brückl, E., Behm, M., Chwatal, W., 2003. The application of signal detection and stacking techniques to refraction seismic data. Oral Presentation at AGU, San Francisco, 08-12 Dec 2003.
Chwatal, W., Kirschner, H., Brückl, E., Zangerl, C., 2006. Kinematics and Hazard of the Niedergallmigg-Matekopf mass movement. EGU General Assembly, Vienna, Austria. Geophysical Research Abstracts vol. 8, p. 05998.
Cruden, D.M., Varnes, D.J., 1996. Landslide types and processes. In: Turner, A.K., Schuster, R.L. (Eds.), Landslides: Investigation and mitigation, pp. 36–75 (Washington).
Eberhardt, E., Bonzanigo, L., Loew, S., 2007. Long-term investigation of a deep-seated creeping landslide in crystalline rock – Part 2: Mitigation measures at Campo Vallemaggia and numerical modelling of deep drainage. Can. Geotech. J. 44, 1181–1199.
Glastonbury, J., Fell, R., 2008. Geotechnical characteristics of large slow, very slow, and extremely slow landslides. Can. Geotech. J. 45, 984–1005.
Guglielmia, Y., Bertranda, C., Compagnona, F., Follaccib, J.P., Mudrya, J., 2000. Acquisition of water chemistry in a mobile fissured basement massif: its role in the hydrogeological knowledge of the La Clapière landslide (Mercantour massif, southern Alps, France). J. Hydrol. 229, 138–148.
Helmstetter, A., Sornette, D., Grasso, J.R., Andersen, J.V., Gluzman, S., Pisarenko, V., 2004. Slider block friction model for landslides: Application to Vaiont and La Clapière landslides. J. Geophys. Res. 109, 1–15.
Hole, J.A., 1992. Nonlinear high-resolution three-dimensional seismic travel time tomography. J. Geophys. Res. 97, 6553–6562.
Itasca, 2007. UDEC – Universal Distinct Element Code, Version 5.0. Itasca Consulting Group, Inc., Minneapolis.
Loew, S., Strauhal, T., 2013. Pore pressure distributions in brittle translational rockslides. International Conference on Vajont 1963-2013 – thoughts and analyses after 50 years since the catastrophic landslide. Italian Journal of Engineering Geology and Environment, Book Series (6), pp. 181–191.
Loew, S., Strauhal, T., 2014. Pore pressure transients in brittle translational rockslides. In: Sassa, K., Canuti, P., Yin, Y. (Eds.), Landslide Science for a Safer Geoenvironment vol. 3. Springer, pp. 115–122.
Noverraz, F., 1996. Sagging or deep-seated creep: fiction or reality? In: Senneset, K. (Ed.), 7th International symposium on landslides. Balkema, Rotterdam, pp. 821–828
Rittinger, P., 1997. Ermittlung der Verschiebungen eines Festpunktfeldes im Oberinntal GPS. University of Innsbruck, Austria (diploma thesis).
Sjörberg, J., 2000. Failure mechanisms for high slopes in hard rock. In: Hustrulid, W.A., McCarter, M.K., Van Zyl, D.J.A. (Eds.), Slope stability in surface mining. SME Society for Mining, Metallurgy, and Exploration, pp. 71–80.
Skempton, A.W., 1964. Long-term stability of clay slopes. Geotechnique 14 (2), 75–101.
Skempton, A.W., 1985. Residual strength of clays in landslides, folded strata and the laboratory. Geotechnique 35, 3–18.
Stark, T.D., Eid, H.T., 1998. Performance of three-dimensional slope stability methods in practice. J. Geotech. Geoenviron. 124, 1049–1060.
Strauhal, T., 2009. Mineralogische und geotechnische Eigenschaften von tektonisch- und massenbewegungsbedingten Kakiriten. University of Innsbruck, Austria (diploma thesis).
Tschada, H., Hofer, B., 1990. Total solids load from catchment area of the Kaunertal hydroelectric power station: the results of 25 years of operation. Hydrology in mountainous regions II – Artificial reservoirs, water and slopes. IAHS Publ. no. 194, pp. 121–128.
Watkins, J.S., Walters, L.A., Godso, L.A., 1972. Dependence of in-situ compressional wave velocity on porosity in unsaturated rocks. Geophysics 37, 29–35.
Watson, A.D., Moore, D.P., Stewart, T.W., Psutka, J.F., 2007. Investigations and monitoring of rock slopes at Checkerboard Creek and Little Chief Slide. In: Eberhardt, E., Stead, D., Morrision, T. (Eds.), Proceeding of the 1st Canada - U.S. Rock Mechanics Symposium, Vancouver, Canada 2. Taylor & Francis Group, pp. 901–908.
Zangerl, C., Prager, C., 2008. Influence of geological structures on failure initiation, internal deformation and kinematics of rock slides. 42nd US Rock Mechanics Symposium and 2nd US-Canada Rock Mechanics Symposium, San Francisco. American Rock Mechanics Association, Curran Associates, Inc., pp. 1–13 (paper 08-063).
Zangerl, C., Prager, C., Chwatal, W., Mertl, S., Renk, D., Schneider-Muntau, B., Eberhardt, E., Kirschner, H., Brandner, R., Brückl, E., Fellin, W., Tentschert, E., Eder, S., Poscher, G., Schönlaub, H., 2009. Landslide failure and deformation mechanisms, investigation and monitoring methods. In: Veulliet, E., Stötter, J., Weck-Hannemann, H. (Eds.), Sustainable natural hazard management in alpine environments. Springer, pp. 135–173.
Zangerl, C., Eberhardt, E., Perzlmaier, S., 2010a. Kinematic behaviour and velocity characteristics of a complex deep-seated crystalline rockslide system in relation to its interaction with a dam reservoir. Eng. Geol. 112, 53–67.
Zangerl, C., Prager, C., Engl, D.A., 2010b. Self-stabilisation mechanisms of slow rock slides in crystalline bedrock (Tyrol, Austria). In: Williams, A.L., Pinches, G.M., Chin, C.Y., McMorran, T.J., Massey, C.I. (Eds.), Geologically Active, 11th Congress of the International Association for Engineering Geology and the Environment (IAEG). Taylor & Francis Group, Auckland, New Zealand, pp. 903–910.
Zangerl, C., Prager, C., Chwatal, W., Brückl, E., Kirschner, H., Brandner, R., 2012. Kinematics and internal deformation of a deep-seated slow rock slide in metamorphic rock (Niedergallmigg, Austria). In: Eberhardt, E., Froese, C., Turner, A.K., Leroueil, S. (Eds.), 11th International & 2nd North American Symposium on Landslides (ISL-NASL 2012), Banff, Canada. Landslides and Engineered Slopes vol. 1. Taylor & Francis Group, pp. 653–658.
Zangerl, C., Strauhal, T., Holzmann, M., 2013. Deep-seated slowly moving rock slides in foliated metamorphic rock masses: New findings about kinematical and hydromechanical processes. EGU General Assembly 2013, Vienna, Austria. Geophysical Research Abstracts vol. 15, p. 7046.
Zangerl C., Holzmann M., Perzlmaier S., Engl D., Strauhal T., Prager C., Steinacher R., Molterer S. 2015: Characterisation and Kinematics of Deep-Seated Rockslides in Foliated Metamorphic Rock Masses. Lollino, G., Giordan, D., Crosta, G.B., Corominas, J., Azzam, R., Wasowski, J., Sciarra, N. (Eds.), Engineering Geology for Society and Territory – vol. 2, Springer International Publishing Switzerland 2014, pp. 571–575.
Zischinsky, U., 1969. Über Sackungen. Rock Mech. 1, 30–52.